JACS
JOURNAL OF THE AMERICAN CHEMICAL SOCIETY
Article
pubs.acs.org/JACS

Singlet Exciton Fission in Polycrystalline Thin Films of a Slip-Stacked Perylenediimide

Samuel W. Eaton,[†] Leah E. Shoer,[†] Steven D. Karlen,[†] Scott M. Dyar,[†] Eric A. Margulies,[†] Brad S. Veldkamp,[†] Charusheela Ramanan,[†] Daniel A. Hartzler,[‡] Sergei Savikhin,[‡] Tobin J. Marks,[†] and Michael R. Wasielewski*[,†]

[†]Department of Chemistry and Argonne-Northwestern Solar Energy Research (ANSER) Center, Northwestern University, 2145 Sheridan Road, Evanston, Illinois 60208-3113, United States

[‡]Department of Physics, Purdue University, 525 Northwestern Avenue, West Lafayette, Indiana 47907, United States

Supporting Information

ABSTRACT: The crystal structure of *N*,*N*-bis(*n*-octyl)-2,5,8,11-tetraphenylperylene-3,4:9,10-bis(dicarboximide), **1**, obtained by X-ray diffraction reveals that **1** has a nearly planar perylene core and $\pi-\pi$ stacks at a 3.5 Å interplanar distance in well-separated slip-stacked columns. Theory predicts that slip-stacked, $\pi-\pi$-stacked structures should enhance interchromophore electronic coupling and thus favor singlet exciton fission. Photoexcitation of vapor-deposited polycrystalline 188 nm thick films of **1** results in a 140 ± 20% yield of triplet excitons (^{3}*$\mathbf{1}$) in τ_{SF} = 180 ± 10 ps. These results illustrate a design strategy for producing perylenediimide and related rylene derivatives that have the optimized interchromophore electronic interactions which promote high-yield singlet exciton fission for potentially enhancing organic solar cell performance and charge separation in systems for artificial photosynthesis.

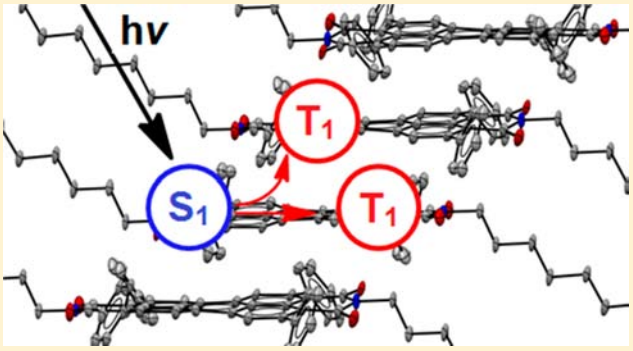

INTRODUCTION

Singlet exciton fission (SF) is the process by which a singlet exciton in a molecular material is energetically down-converted into two independent triplet excitons.[1] Thermodynamic modeling predicts that using an SF material in a single-junction solar cell could theoretically increase the Shockley–Queisser limit for power conversion efficiency from 32% to 44%, assuming that SF results in the formation of two triplet excitons, each of which produces an electron–hole pair quantitatively.[2] Another potentially important advantage of using SF materials in solar cells is that charge recombination of the initially formed triplet electron–hole pairs to the singlet ground state is a spin-forbidden process, such that solar cell efficiency losses due to charge recombination should be reduced.

SF was first proposed in 1965 to explain delayed fluorescence in anthracene crystals,[3] then invoked in crystalline tetracene to rationalize its low fluorescence quantum yield, and subsequently confirmed in pentacene crystals.[4] SF has been observed in mixed crystals (heterofission) of anthracene doped with tetracene[5] and pentacene doped with tetracene.[4b] More recently, tetracene,[6] pentacene,[6d,7] *p*-terphenyl and *p*-sexiphenyl,[8] tetracyano-*p*-quinodimethane,[17,18] 1,3-diphenylisobenzofuran,[9] perylene,[10] benzophenone,[11] and rubrene[12] have all been shown to have SF triplet quantum yields (Φ_T) ranging from 6% to 200%. SF has also been observed in carotenoid aggregates with high quantum efficiency[13] and in selected aromatic polymers,[14] while it has been discounted in poly-*p*-phenylenes.[15] Despite significant computational work to predict the optimal molecular structures for SF,[16] only one designer SF chromophore has thus far been reported.[9] Although there are a few recent reports that explore SF in molecular photovoltaic devices,[17] SF materials have not been widely used in such devices because the factors that control SF efficiency in molecular materials are poorly understood.

In the simplest kinetic scheme, the conversion of a singlet exciton into two triplet excitons can be written as[18]

$$S_0 + S_1 \underset{-k_d}{\overset{k_d}{\rightleftharpoons}} {}^1(TT) \underset{k_{TTA}}{\overset{k_{SF}}{\rightleftharpoons}} T_1 + T_1 \qquad (1)$$

where k_d describes the coupling of the singlet to the correlated triplet pair ^{1}(TT), k_{SF} is the rate of SF, and k_{TTA} is the rate of triplet–triplet annihilation. Achieving optimized SF yields requires among other factors that the sum of the energies of the two triplet excitons (T_1) is lower than the energy of the vibrationally relaxed singlet state (S_1), i.e., $E(S_1) > 2E(T_1)$ (Scheme 1). This requirement is not easy to fulfill because in most common chromophores the $E(S_1) - E(T_1)$ gap is considerably smaller than the $E(T_1) - E(S_0)$ gap. Furthermore,

Received: May 31, 2013
Published: September 6, 2013

   dx.doi.org/10.1021/ja4053174 | J. Am. Chem. Soc. 2013, 135, 14701–14712

Scheme 1. Energy Level Diagram for Singlet Exciton Fission between Two Interacting Molecules, A and B

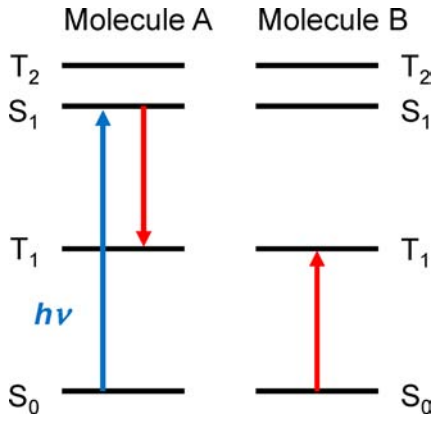

T_1–T_1 annihilation is potentially a serious problem in dimers and small oligomers, in which the triplet excitons cannot diffuse apart, as they can in crystals. If $E(S_1) > 2E(T_1)$, the T_1–T_1 annihilation rate to yield S_1 and S_0 is slow because it is endogonic (k_{TTA}). Annihilation leading to $S_0 + S_0$ is also likely to be slow because it is very exergonic and occurs in the Marcus inverted region.[19] T_1–T_1 annihilation to yield the next higher triplet T_2 and S_0 could also be nearly isoenergetic and very fast. Therefore, it is desirable that $E(T_2) > 2E(T_1)$ to guarantee that this annihilation process is endogonic and slow. Thus, optimal SF chromophores should satisfy the condition $E(S_1)$, $E(T_2) > 2E(T_1)$ (Scheme 1).

In addition to the aforementioned energetic requirements, it is clear that intermolecular electronic coupling and orientation are also critical for efficient SF, but only two series of systematic studies varying these parameters have been reported.[9,16b,20] The present work highlights the delicate balance among molecular geometry, electronic coupling, and SF efficiency. It has been suggested that a cofacial, π–π slip-stacked relationship between molecular chromophores may facilitate high SF efficiency.[1] This is a consequence of the requirement to prevent cancellation of the electron repulsion integrals involving the HOMOs and LUMOs of the two chromophores that contribute to the overall matrix element for the SF process.

Perylene-3,4:9,10-bis(dicarboximide) (PDI) and its derivatives have attracted great interest as visible chromophores for energy and charge transport studies,[21] especially with regard to potential applications as visible light-absorbing electron acceptors in organic photovoltaics.[22] Not only are PDIs more thermally and photochemically stable than most other molecules currently being explored for SF,[23] they also exhibit a strong propensity to self-organize into ordered assemblies, both in solution and in the solid state via π–π stacking interactions, often aided by hydrogen-bonding and nano/microsegregation.[21a,c–u,24] Ford and Kamat reported that the lowest triplet-state energy of PDI (E_T) is approximately 1.2 eV, about half that of its singlet energy (E_S = 2.34 eV), and that the quantum yield of ^{3}*PDI by direct excitation is $<10^{-3}$.[25] Recently, a weak phosphorescence spectrum of ^{3}*PDI was reported, which yields E_T = 1.1 eV.[26] Also, TD-DFT calculations at the 6-31G(d) level of theory give $E(T_2)$ = 2.69 eV (see the Supporting Information), so PDI comes close to satisfying the energetic requirements for SF: $E(T_2)$, $E(S_1) > 2E(T_1)$. PDI derivatives have distinct advantages over currently known molecules that undergo SF because, unlike chromophores that absorb at shorter wavelengths, PDI derivatives absorb light strongly in the middle of the visible spectrum, so the ^{3}*PDI energy is sufficiently high that hole injection from ^{3}*PDI into semiconductors should be facile.

Many early measurements of SF relied on steady-state optical methods for triplet detection, which suffer from the inability to determine what fraction of the triplet yield is due to SF. More recent work uses time-resolved optical methods to detect SF that can differentiate between ultrafast triplet formation by SF and conventional triplet formation by spin–orbit-induced intersystem crossing (SO-ISC).[6,7,9a,12c,13a,b,14d,17a,20a,b,27] Herein we report the photophysics of polycrystalline thin films of *N*,*N*-bis(*n*-octyl)-2,5,8,11-tetraphenyl-PDI, **1**. The crystal structure of **1** obtained by X-ray diffraction reveals segregated, slip-stacked columns of **1** that are π–π stacked at a 3.5 Å interplanar distance. Femtosecond transient absorption spectroscopy on vapor-deposited thin films of **1** demonstrates ^{3}***1** formation as a result of SF. These results illustrate an attractive design strategy for producing PDI derivatives that can undergo SF and find potential applications in enhancing solar cell performance.

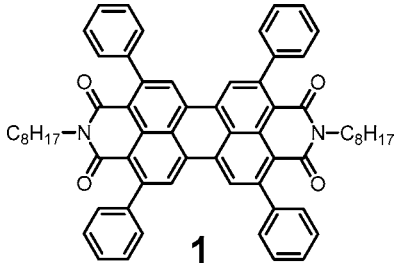

1

EXPERIMENTAL SECTION

Synthesis. The synthesis and characterization of **1** are described in the Supporting Information. The final product was purified by gradient sublimation at 350 °C and 10^{-6} Torr.

Crystallography. Single crystals of **1** were grown by slow diffusion of heptane into a chloroform solution of **1**. These crystals were mounted with Paratone oil on glass capillaries and placed in the nitrogen cold stream (100 K) of a Bruker AXS APEX2 diffractometer equipped with a charge-coupled device (CCD) detector and an IμS Cu Kα microfocus source with MX optics. All data were corrected for absorption via SADABS. Structures were solved and refined using SHELXTL.

Thin Film Fabrication and Characterization. All vapor deposition was performed with a Cooke Vacuum Products organic vapor depositor. The approximate film thickness was monitored in situ using an in-chamber quartz-crystal microbalance. Films of **1** were vapor deposited on heated (383 K) Arrayit Super Clean 2 glass substrates under a vacuum of 3×10^{-6} Torr (0.8 Å/s). Film thicknesses were measured in triplicate by profilometry using a Veeco Dektak 150 surface profiler. Powder X-ray diffraction (PXRD) measurements on the films were performed using a Rigaku ATX-G thin-film diffraction workstation in grazing incidence geometry (0.2° incident angle). All PXRD diffractograms were background subtracted using the glass substrates. The experimental PXRD pattern was fit using the Le Bail approach performed in GSAS.[28] After background subtraction, the fit was seeded with lattice parameters obtained from the single-crystal structure, and the peak intensities, lattice parameters, and peak profiles were refined sequentially.

Photophysical Measurements. Steady-state absorbance spectra were obtained with a Shimadzu 1800 spectrophotometer, and fluorescence measurements were carried out with a PTI QuantaMaster 1 single-photon spectrofluorimeter in right-angle configuration. Femtosecond transient absorption (fsTA) measurements were made using a regeneratively amplified Ti:sapphire laser system operating at

dx.doi.org/10.1021/ja4053174 | J. Am. Chem. Soc. 2013, 135, 14701–14712

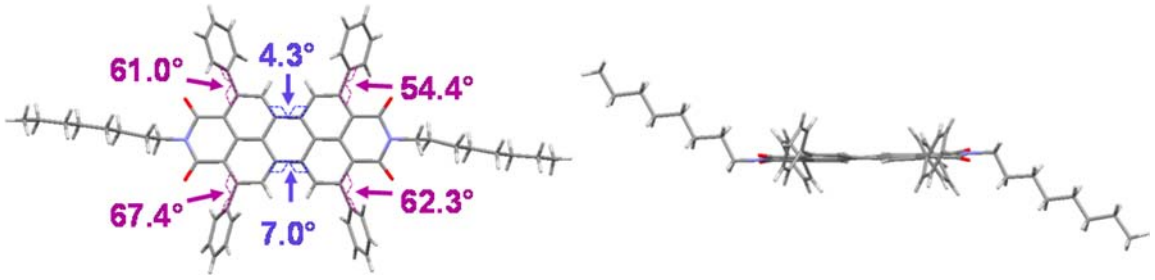

Figure 1. Asymmetric unit of structure of PDI molecule **1** with selected torsion angles indicated.

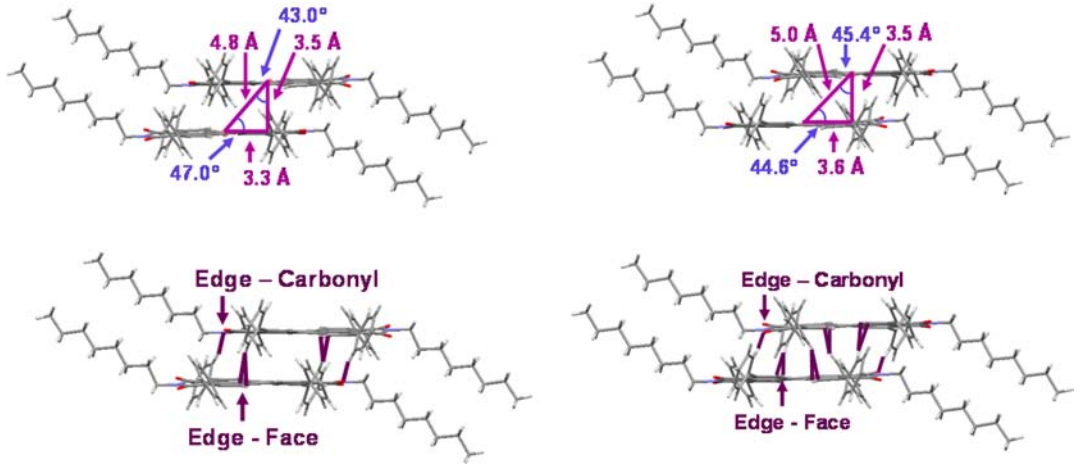

Figure 2. Molecular packing distances and angles for PDI molecule **1**: left, within a unit cell; right, between unit cells.

832 nm and a 1 kHz repetition rate as described previously.[29] The output of the amplifier was frequency-doubled to 416 nm using a 200 μm thick lithium triborate crystal to produce 120 fs excitation pulses. A small portion of the fundamental was focused onto a sapphire disk to generate the white-light probe spanning 440−800 nm. Spectral and kinetic data were collected with a CCD array detector and a 6 ns pump−probe delay track. Solution samples had an absorbance of 0.9 at the excitation wavelength and were irradiated in 2 mm quartz cuvettes with 1 μJ/pulse focused to a 0.5 mm diameter spot. fsTA spectroscopy on the thin films was performed with the pump beam focused to a 1 mm diameter spot size on the films that was matched to the diameter of the white light probe pulse. The pump pulse energy was varied as given in the caption of Figure 8 to study the effect of the excitation density on singlet fission dynamics. The total instrument response function (IRF) was 180 fs. Transient spectra were averaged for 10 s. Each three-dimensional ΔA vs time and wavelength data set was analyzed by singular value decomposition and subsequent global fitting[30] of the principal kinetic components to a model that takes into account singlet−singlet annihilation of a pair of excitons,[31] which is competitive with singlet fission:

$$-\frac{d[S_1]}{dt} = \frac{k_{SSA}}{2}[S_1]^2 + k_{SF}[S_1] \quad (2)$$

$$\frac{d[T_1]}{dt} = 2k_{SF}[S_1] \quad (3)$$

where k_{SSA} and k_{SF} are the rate constants for singlet−singlet annihilation and singlet fission, respectively. In addition to the rate constants, the analysis yields the species-associated transient absorption difference spectra for the excited singlet exciton, $A(S_1) - A(S_0)$, and the triplet exciton, $A(T_1) - A(S_0)$. The analysis was implemented in MATLAB[32] and uses a constrained interior point algorithm to obtain a nonlinear least-squares fit.

The nanosecond TA (nsTA) apparatus has been described previously.[33] nsTA experiments on **1** were performed on the same thin films used for the fsTA experiments using 7 ns, 416 nm laser pulses having the energies indicated in the figures and apertured to 1.0 cm diameter spot sizes at the samples. The solution samples were degassed using five freeze−pump−thaw cycles. Analysis of kinetic data was performed at multiple wavelengths using a Levenberg−Marquardt nonlinear least-squares fit to a general sum-of-exponentials function with a Gaussian convolution to account for the finite instrument response.

Picosecond time-resolved fluorescence (TRF) measurements were made using a streak camera system (Hamamatsu C4780 Streakscope). Excitation pulses at 416 nm were generated using a laboratory-built, cavity-dumped, Ti:sapphire laser system (center wavelength, 832 nm; spectral width, 55 nm; pulse duration, 25 fs; repetition rate, 820 kHz) followed by frequency doubling in a 200 μm thick lithium triborate crystal. A parabolic mirror was used to focus the excitation beam into the sample, and the subsequent fluorescence was collected in a backscattering geometry using the same parabolic mirror. Magic angle detection was used to avoid polarization effects. The IRFs were 750, 370, 180, 85, 44, and 30 ps (fwhm) in the 50, 20, 10, 5, 2, and 1 ns full-scale time ranges, respectively. All data were acquired in single-photon-counting mode using the Hamamatsu HPD-TA software. Singular value decomposition of the three-dimensional intensity vs time and wavelength data set followed by global fitting yielded the decay-associated fluorescence spectra using Surface Xplorer 1.0 (Ultrafast Systems).[34]

The phosphorescence emission spectra were measured using a laboratory-built, time-gated IR spectrometer capable of detecting weak emission from molecules with phosphorescence quantum yields as low as 10^{-7}. The system is based on the design of Takiff et al.[35] using a liquid nitrogen cooled germanium photodetector (North Coast Scientific, EO-817L). Samples were dissolved in 2-MeTHF, housed in quartz EPR tubes, and loaded into a liquid nitrogen cryostat at 77 K (Oxford Instruments, Optistat DN). Tunable 5 ns, 1 mJ excitation pulses from an optical parametric oscillator (Ekspla, NT 342B) were used to excite the samples. Emission was focused on a fast optical gate consisting of a 10 cm optical chopper wheel (Scitec, 300CD) rotating at 6000 rpm and flanked by slits on both sides to reduce scattered light

dx.doi.org/10.1021/ja4053174 | J. Am. Chem. Soc. 2013, 135, 14701−14712

and enable fast temporal gating (approximately 30 μs transition from closed to open). The gated emission signal was further passed through a 700 nm LWP interference filter and collimated into a monochromator (Oriel, MS257), followed by the germanium detector. Rapid time gating is essential to discriminate the intense but short-lived fluorescence signal from the weak, long-lived phosphorescence.

RESULTS AND DISCUSSION

Structural Analysis. Molecule **1** packs in the triclinic space group $P\bar{1}$ with one molecule representing the asymmetric unit and two molecules per unit cell; the primary crystallographic parameters are found in Tables S1 and S2 in the Supporting Information. The asymmetric unit of **1** shows the PDI core to be roughly flat with dihedral angles of 4.3° and 7.0° for the four carbon planes comprising each of the bay regions (Figure 1). Furthermore, the planes of the phenyl groups at the 2,5,8,11-skeletal positions are twisted 54.5−67.4° out of the PDI mean plane (Figure 1). The *n*-octyl groups are fully extended with all of the carbons in an *all-trans* conformation (Figure 1).

The PDI molecules in the single crystals of **1** form slipped stacks with a PDI−PDI face-to-face distance of 3.5 Å and neighboring molecules slipped by 3.3 Å within the unit cell and 3.6 Å between unit cells (Figure 2). The offset angle between the PDI molecules is 44.6−47°, placing the alignment in the *J*-aggregate regime, but close to the magic angle.[36] There is also a small offset of 0.2 Å (87°) along the transverse molecular axis. There are several intermolecular interactions that are less than the sum of van der Waals radii; all of these involve the four phenyl groups and the phenyl edge to either PDI face or carbonyl oxygen (Figure 2).

The phenyl groups on the periphery of PDI molecule **1** form edge-to-face chains (Figure 3). The *n*-octyl groups are fully

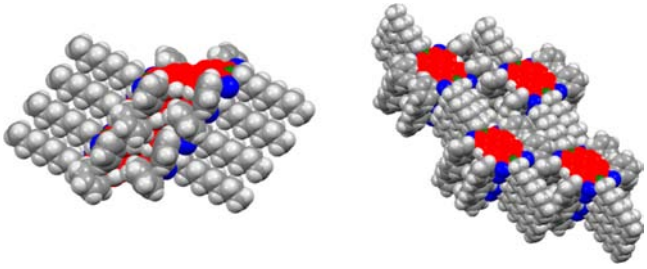

Figure 3. Space-filling packing diagrams of PDI molecule **1**.

extended and aligned parallel to the alkyl chains of neighboring molecules, thus maximizing their van der Waals contacts. Due to steric interactions of the phenyl groups, **1** $\pi-\pi$ stacks in a slip-stacked geometry. The $\pi-\pi$ stacks pack with the alkyl chain of one molecule aligning along the perpendicular to the *para* hydrogen of the phenyl groups, thus preventing any interdigitation from the side of the molecule (Figure 3).

Thin films of **1** were vapor-deposited on glass substrates held at 383 K during deposition and were 188 ± 7 nm thick as determined by profilometry (Figure S1, Supporting Information). PXRD measurements on the films show that they are polycrystalline (Figure 4), while the calculated XRD diffractogram (Figure S2, Supporting Information) generated from the single-crystal structure described above allows us to assign the major peak (5.6°) and minor peak (7.7°) to the (001) and (010) reflections, respectively. The lattice parameters for the polymorph in the polycrystalline films were obtained from the PXRD data using the GSAS program. The fit to the data shows that the unit cell parameters of **1** change somewhat when

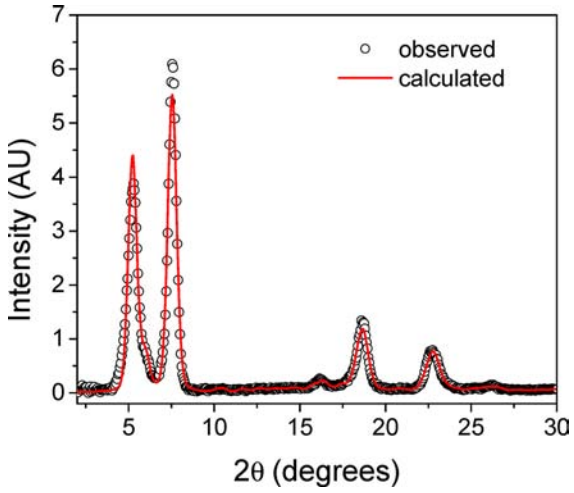

Figure 4. PXRD diffractogram of a film of **1** deposited at 383 K. The diffractogram was obtained at 295 K, and fit parameters to the data were obtained using the GSAS program to give the unit cell parameters.

moving from the single crystal to the film primarily because the single-crystal XRD data and the PXRD film data were acquired at 100 and 295 K, respectively (Table 1). Temperature-dependent changes in the lattice parameters orthogonal to the PDI stacking direction in *N*,*N*-bis(phenethyl)-PDI single crystals have been observed previously.[37] Assuming that the aromatic core structure of **1** does not change significantly with temperature, the observed changes in lattice parameters can be used to estimate how the relative distances between the two PDI molecules within the unit cell change in going from the single crystal to the film. The two PDI molecules in the unit cell are rotated significantly away from the unit cell axes, so a rotational transformation was performed to obtain the changes in PDI−PDI spacing. In going from the single crystal at 100 K to the film at 295 K, the PDI long (N−N) axis slips by an additional 0.45 Å, the short axis slips by an additional 0.1 Å, and the average $\pi-\pi$ distance increases by 0.18 Å. These changes can be viewed as an upper limit because the changes in lattice spacing may simply involve the more flexible *n*-octyl chains. Thus, the slip-stacked $\pi-\pi$ interactions indicated by the single-crystal structure are maintained in the vapor-deposited films.

Table 1. Comparison of the Unit Cell Parameters Obtained from XRD on a Single Crystal of 1 and PXRD Measured at 295 K of a 188 nm Film of 1 Deposited at 383 K[a]

	single-crystal XRD (100 K)	film PXRD fit (295 K)	difference
a (Å)	9.8742(11)	9.491(17)	−0.383
b (Å)	15.5304(17)	15.441(14)	−0.089
c (Å)	16.387(3)	17.240(14)	+0.853
α (deg)	93.643(11)	92.50(8)	−1.143
β (deg)	99.206(11)	100.21(15)	+1.004
γ (deg)	105.959(8)	105.54(11)	−0.419

[a]The parameters fit to the PXRD data were obtained using the GSAS program to give the unit cell parameters.

Steady-State Photophysics. The steady-state UV−vis absorption spectrum of **1** in toluene is compared to that of the vapor-deposited film in Figure 5. The film spectrum exhibits intensity changes as well as broadening and red shifting, resulting in maxima at 462 and 573 nm. The spectrum of **1** in

dx.doi.org/10.1021/ja4053174 | J. Am. Chem. Soc. 2013, 135, 14701−14712

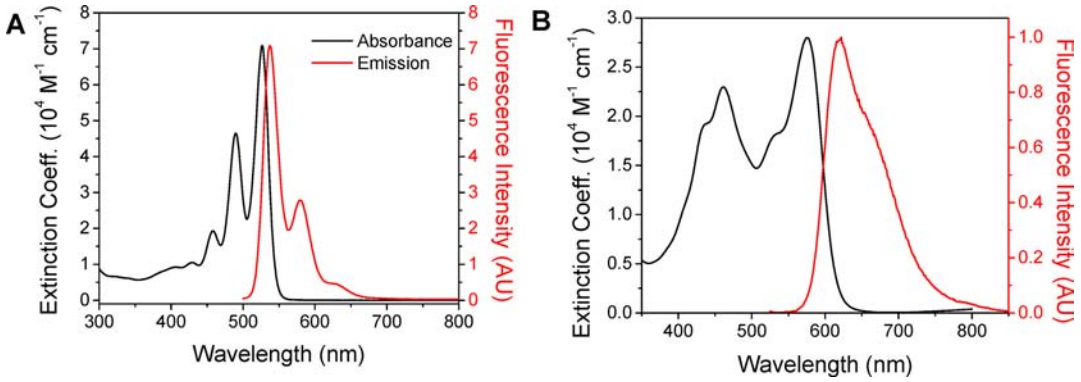

Figure 5. UV−vis absorption and fluorescence spectra of PDI molecule **1**: (A) in CH_2Cl_2, fluorescence excited at 490 nm, (B) a 188 nm thick film of **1**, fluorescence excited at 460 nm. The fluorescence spectra are normalized to the absorption spectra.

the film strongly resembles those of *N*,*N*-dimethyl-PDI and *N*,*N*-bis(phenethyl)-PDI,[37,38] which are known to crystallize in $\pi-\pi$ slip-stacked geometries similar to that of **1**. Theoretical analyses of these spectra have questioned the role of charge transfer (CT) states in addition to Frenkel excitons in describing the electronic states of these PDI derivatives in the solid state.[39] However, recent computational studies at a high level of theory indicate that the 462 nm band can be assigned to the $S_0 \rightarrow S_2$ transition, which is considerably enhanced and red-shifted in the solid relative to the corresponding monomer in solution, while the 573 nm band is assigned to the $S_0 \rightarrow S_1$ transition, which is also red-shifted relative to the monomer transition at 525 nm.[40]

The fluorescence spectrum of **1** in the film occurs at 616 nm and mirrors the absorption spectrum of **1** in the film (Figure 5B). The energy-averaged maxima of the absorption and emission spectra of **1** in the thin film yield E_{S1} = 2.08 eV, whereas in solution E_{S1} = 2.34 eV.

Phosphorescence spectra for **1** were obtained at 77 K using the high-sensitivity apparatus described in the Experimental Section. Figure S3 in the Supporting Information shows that cooling a solution of **1** in 2-MeTHF to 77 K results in a UV−vis absorption spectrum that displays absorption features characteristic of both monomeric **1** (Figure 5A) and the slipped-stacked structure (Figure 5B), indicating that a mixture of these species exists in the low-temperature glass. Selective excitation of the monomer absorption at 535 nm results in a phosphorescence spectrum with a maximum at 970 nm (1.28 eV), whereas selective excitation of the slip-stacked structure at 580 nm reveals a spectrum with a maximum at 1090 nm (1.14 eV) (Figure 6). These data show that $\pi-\pi$ slip-stacking of **1** results in stabilization of its triplet exciton energy by 0.14 eV, which is slightly more than half the 0.26 eV stabilization observed for its corresponding singlet exciton (Figure 5). Computational studies predict that the electronic coupling between a singlet exciton and neighboring ground-state molecules is often much larger than that of the corresponding triplet exciton.[16e] In contrast, the stabilization of the triplet exciton of **1** by interaction with neighboring molecules of **1** is relatively large compared to the corresponding singlet exciton stabilization. Comparing the value of $E(S_1)$ = 2.08 eV for **1** in the polycrystalline solid with the measured triplet energy $E(T_1)$ = 1.14 eV for aggregated **1** in 2-MeTHF at 77K, SF in films of **1** should be endothermic by 0.2 eV. This modest endothermicity is similar to that observed for tetracene, which nevertheless undergoes SF in nearly 200% yield.[6] Recent observations by

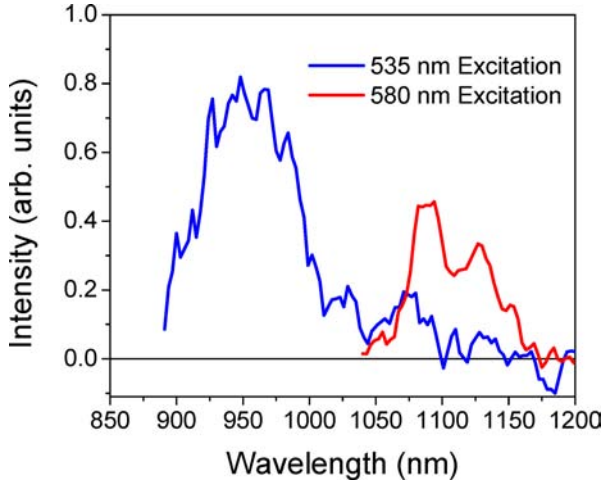

Figure 6. Phosphorescence spectra of PDI molecule **1** in 2-MeTHF at 77 K.

Zhu and co-workers have attributed the temperature-independent high SF yield in tetracene to coherent coupling of the excited singlet state to the multiexciton state and a favorable entropy change for SF, which makes the overall SF processes exergonic.[6b]

Transient Emission and Absorption Measurements. The time-resolved fluorescence decay of **1** in the film shows three components, 210 ± 20 ps (0.75), 870 ± 130 ps (0.11), and 2.5 ± 0.8 ns (0.03) (Figure 7A). The data were obtained with a low excitation density (excitons per cm^3) of 2.2×10^{16} cm^{-3} to avoid singlet−singlet annihilation. Singular value decomposition and global fitting of the data were used to obtain more accurate decay times and their decay-associated spectra (Figure 7B). This latter analysis agrees well with the fsTA data presented below. The spectrum of the shortest decay component matches that of the steady-state spectrum of **1** in the film, while the spectra of the 940 ps and 2.0 ns components are red-shifted with broad maxima at 664 and 675 nm, respectively. These spectra are most likely a result of excimer-like emission from defect sites within the polycrystalline film. The 2.0 ns component is attributed to a small amount of delayed fluorescence resulting from triplet−triplet annihilation in the film, leading directly to a second population of excimer-like states having geometries that afford greater stabilization of the excimer-like state as implied by their slightly more red-shifted emission. Due to the low emission yield of the excimer-

dx.doi.org/10.1021/ja4053174 | J. Am. Chem. Soc. 2013, 135, 14701−14712

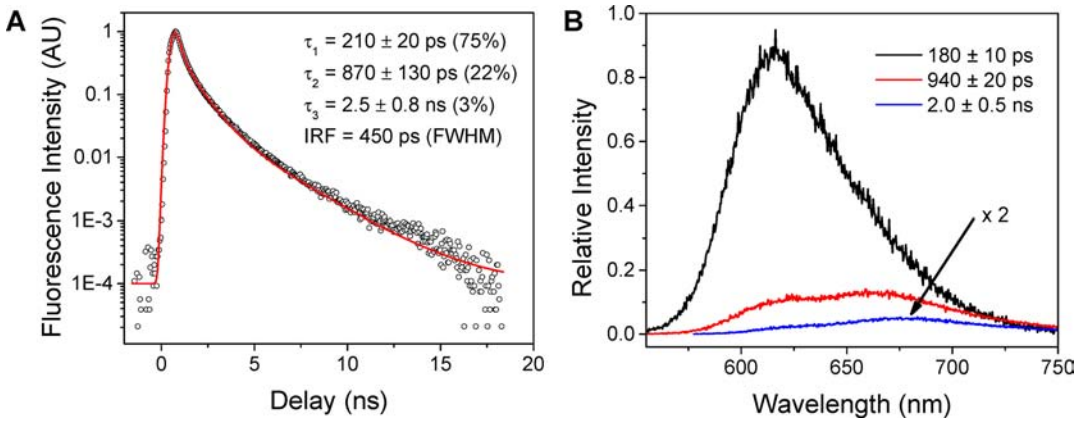

Figure 7. Time-resolved fluorescence data for a 188 nm thin film of PDI molecule **1** excited with a 0.2 nJ, 416 nm laser pulse at a 820 kHz repetition rate (excitation density 2.2×10^{16} cm^{-3}): (A) time-resolved fluorescence decay monitored at 610 nm, (B) decay-associated spectra for the indicated time constants.

like species, and the dynamic range of the measurements, there is no reliable evidence of longer lived components. The fluorescence lifetime of monomeric **1** immobilized in a polystyrene film is ~4 ns at 295 K, which implies that its emission quantum yield in the polycrystalline film is reduced by about a factor of 20.

Figure 8A shows fsTA spectra following photoexcitation of the film of **1** with 120 fs, 416 nm laser pulses having an excitation density of 7.1×10^{18} cm^{-3}. For comparison, on the basis of the crystallographic data, the number density of **1** in the solid is 8.4×10^{20} cm^{-3}, so the number of excitons produced in the solid film is relatively low. Ground-state bleaching at 590 nm as well as 480−550 and 640−800 nm transient absorption features appear within the IRF and are attributed to formation of ^{1}*$\mathbf{1}$.[41] The three-dimensional fsTA data set of ΔA vs time (0−6 ns) and wavelength (480−800 nm) was analyzed using singular value decomposition (SVD) and subsequent global fitting of the principal kinetic components to the model described in eqs 2 and 3 to yield reaction rate constants as well as the relevant species-associated spectra (Figure 8B,D,F,H).[34]

The model produces two spectra clearly identified with the $A(S_1) - A(S_0)$ and $A(T_1) - A(S_0)$ transient absorption difference spectra, where $A(S_1)$, $A(T_1)$, and $A(S_0)$ are the absorbances of S_1, T_1, and S_0, respectively. In all cases, the $A(S_1) - A(S_0)$ transient spectra have a strong bleach at 590 nm and a broad absorption at 620−800 nm. This bleach persists in the $A(T_1) - A(S_0)$ transient spectra, whereas the near-infrared absorption is much weaker. The decay of the $A(S_1) - A(S_0)$ spectrum is dominated by singlet−singlet annihilation, which occurs with $k_{SSA} = 5.8 \times 10^{12}$ M^{-1} s^{-1} (or 9.3×10^{-9} cm^3 s^{-1}), which is similar to the rates observed for closely packed chlorophylls in photosynthetic light-harvesting proteins.[31] In contrast, the $A(T_1) - A(S_0)$ spectrum rises with $k_{SF} = (5.6 \pm 0.2) \times 10^9$ s^{-1} or $\tau_{SF} = 180 \pm 10$ ps and lives for $\tau \gg 6$ ns. The data show that lowering the excitation density to only 7.1×10^{17} cm^{-3} (Figure 8G,H), where the ratio of ground-state molecules to excited molecules is ~1000:1, results in somewhat less singlet−singlet annhilation, yet it still competes effectively with SF. Nevertheless, a comparison of the SF time constant ($\tau_{SF} = 180 \pm 10$ ps) obtained from modeling the fsTA data on the films of **1** with the time constant for the principal fluorescence lifetime component ($\tau_F = 180 \pm 10$ ps) reveals that these numbers are identical within experimental error. The excitation density for the fluorescence measurement is only 2.2 $\times 10^{16}$ cm^{-3}, and the fluorescence lifetime data analysis yields no resolvable shorter components, so the annihilation-free SF time constant is 180 ps. For comparison, Figure S4 in the Supporting Information shows several single-wavelength kinetic fits to the fsTA data in Figure 8A, which yield kinetic components and amplitudes very similar to those obtained from the global fits.

Triplet-State Characterization. The long-lived (≫6 ns) $A(T_1)-A(S_0)$ transient absorption spectrum was further characterized by performing nsTA on the film of **1** using 7 ns, 416 nm, 1.7 mJ laser pulses (Figure 9A). The nsTA spectra are nearly identical to those obtained by fsTA in Figure 8 and are also similar to the published spectrum of unsubstituted ^{3}*$\mathbf{1}$.[25] The dependence of the magnitude of the nsTA spectra on the excitation density was found to be linear in this range of excitation densities, so singlet−singlet annihilation does not compete kinetically with SF in the nanosecond experiment (Figure 9B).

To determine the influence of the phenyl substituents on the $T_1 \rightarrow T_n$ absorption spectrum of monomeric ^{3}*$\mathbf{1}$, nsTA measurements were also performed on **1** in toluene solution with anthracene added as a triplet sensitizer.[25,42] Following selective photoexcitation of the anthracene at $\lambda_{max} = 355$ nm, the anthracene triplet (^{3}*An) absorption initially observed at 428 nm[25] decays with a time constant $\tau_D = 2.37 \pm 0.01$ μs. This decay is accompanied by the rise in absorption at 450−650 nm, which results from the formation of ^{3}*$\mathbf{1}$ (Figure S5, Supporting Information). Adding the scaled ground-state absorption spectrum of **1** to its nsTA spectrum at 3 μs gives the $T_1 \rightarrow T_n$ spectrum of **1** in toluene (Figure 10A), which agrees well with that reported previously by Ford and Kamat for unsubstituted ^{3}*PDI,[25] except that the 524 nm $T_1 \rightarrow T_n$ absorption maximum of **1** is red-shifted by 19 nm relative to that of unsubstituted PDI. Similarly, the ground-state UV−vis spectrum of the film was scaled and added to that of the nsTA spectrum at 60 ns (Figure 9) to obtain the $T_1 \rightarrow T_n$ absorption spectrum of **1** in the polycrystalline film (Figure 10B). The criterion used to determine how much to scale the ground-state spectrum before adding it to the nsTA spectrum to obtain the $T_1 \rightarrow T_n$ absorption spectrum is minimizing the residual inflection remaining at the wavelength of the ground-state bleach at 590 nm. This is the largest contributor to the error bars on the $T_1 \rightarrow T_n$ extinction coefficient and thus to the triplet yield determination given below. In both solution and in

dx.doi.org/10.1021/ja4053174 | J. Am. Chem. Soc. 2013, 135, 14701−14712

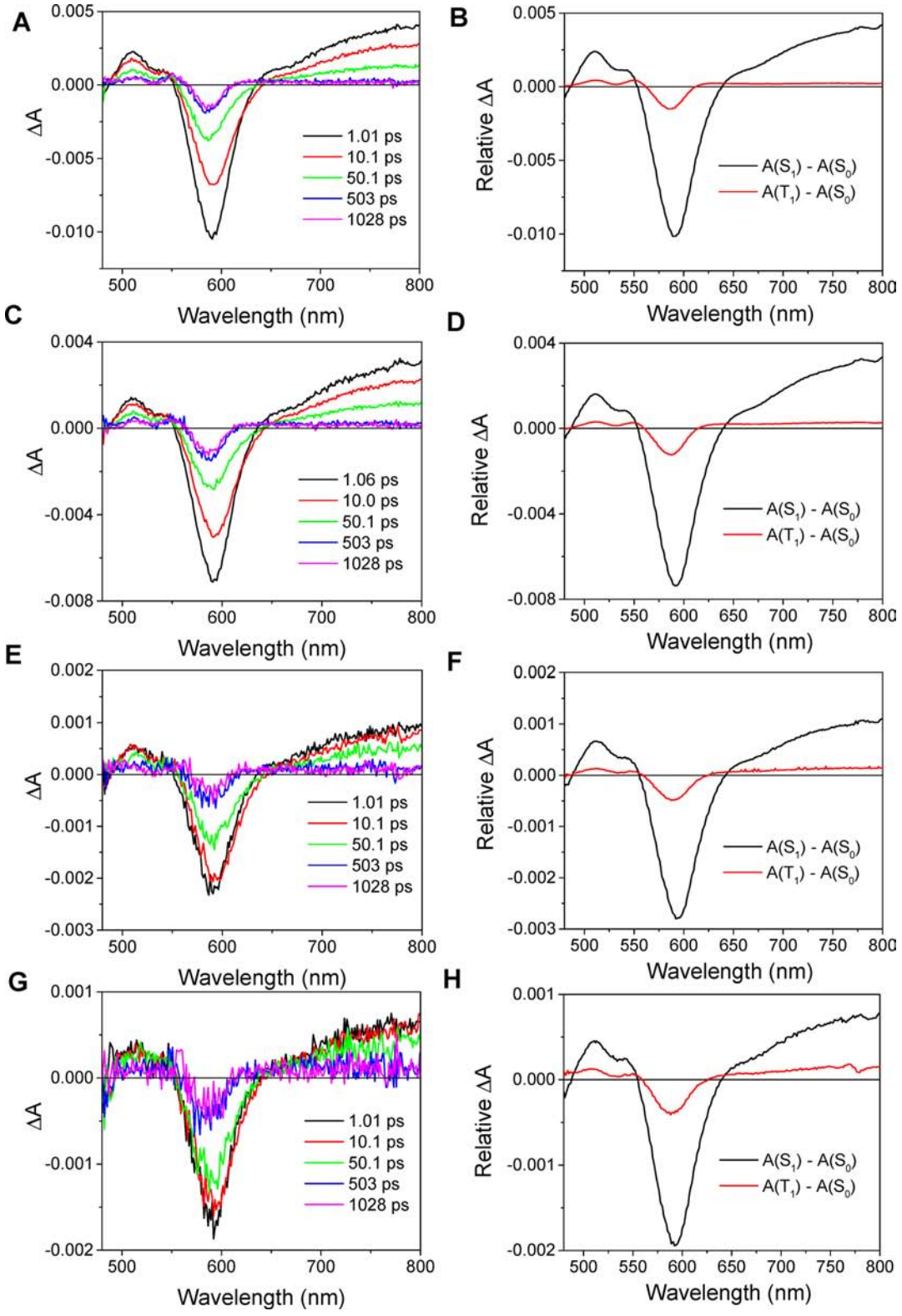

Figure 8. (A, C, E, G) fsTA spectra of a 188 nm film of PDI molecule **1** at the indicated times following 120 fs, 416 nm laser pulses having excitation densities of 7.1×10^{18}, 3.5×10^{18}, 1.4×10^{18}, and 7.1×10^{17} cm^{-3}, respectively. (B, D, F, H) Species-associated spectra obtained from SVD analysis, global fitting, and target analysis of (A), (C), (E), and (G), respectively.

the film there is significant overlap of the $S_0 \rightarrow S_n$ and $T_1 \rightarrow T_n$ spectra of **1**.

The $T_1 \rightarrow T_n$ spectrum of **1** in the film has sharper features and is red-shifted relative to that obtained in solution. It also bears a striking resemblance to the $S_0 \rightarrow S_n$ spectrum of **1** in the film, albeit with a significant blue shift of its lowest energy absorption band. The $S_0 \rightarrow S_n$ and $T_1 \rightarrow T_n$ spectra of a relatively small number of organic single crystals, e.g., anthracene,[43] benzophenone,[44] *p*-terphenyl,[45] *trans*-stilbene,[46] and perylene,[47] have been measured using transient absorption

dx.doi.org/10.1021/ja4053174 | J. Am. Chem. Soc. 2013, 135, 14701−14712

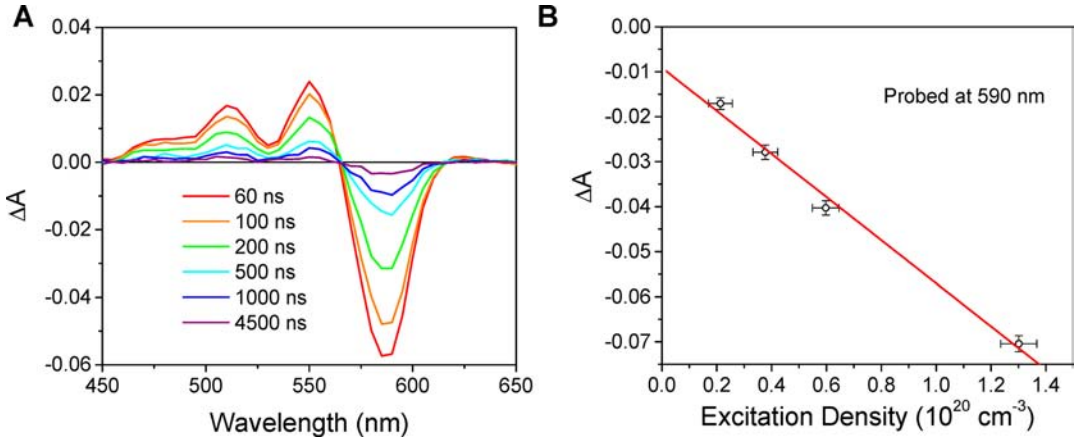

Figure 9. (A) nsTA spectra of a 188 nm film of PDI molecule **1** excited with a 7 ns, 416 nm, 1.7 mJ, 1.0 cm diameter laser pulse (excitation density 1.2×10^{20} cm^{-3}). The glass slide was mounted in a cryostat evacuated to 10^{-2} Torr at 295 K. (B) Excitation density dependence of the transient bleach at 60 ns following a 7 ns, 416 nm laser pulse and the linear fit to the data ($R^2 = 0.988$).

techniques. The spectra observed in single crystals generally appear similar to those measured in solution provided that the interchromophore molecular orientations minimize electronic coupling between them. In contrast, when significant orbital overlap between the chromophores occurs within the crystal, the $S_0 \rightarrow S_n$ and $T_1 \rightarrow T_n$ spectra both show considerable deviations from those in solution. The $S_0 \rightarrow S_n$ spectra often show strong Davydov splitting as well as an overall environmental red shift of the transitions, while the $T_1 \rightarrow T_n$ spectra show a wide variability. This variability for triplet excitons results from the fact that the long-range dipole−dipole contribution to the overall electronic interaction between the triplet exciton and its neighboring chromophores is negligible. Thus, the electronic interaction of the triplet exciton with its neighboring chromophores is largely orbital overlap driven, making the interaction exponentially distance dependent and very sensitive to small structural changes in the solid. For example, the $T_1 \rightarrow T_n$ spectra of both α- and β-perylene crystals have an additional red-shifted band that is not present in solution. This band is broad and featureless in α-perylene, which has two π-stacked perylene molecules, whereas the band is much more structured in β-perylene, in which the $\pi-\pi$ distance is longer.[47c] The authors suggest that these bands may be charge transfer transitions that result from increased electronic coupling in the crystals resulting from the constrained interchromophore orientations.

We speculate that the similarity between the $S_0 \rightarrow S_n$ and $T_1 \rightarrow T_n$ spectra of **1** in the film results from the unusually strong electronic coupling between the triplet exciton of **1** and its neighboring molecules. The triplet exciton spectral width depends on several factors, including the degree of order in the molecular solid and the magnitude of the Davydov splitting.[48] The dipole−dipole contribution to the Davydov splitting is most likely negligible in this case as it is for most triplet excitons,[48] so the sharpening of the spectrum more directly reflects the significant orbital overlap within the one-dimensional π-stacks of **1** illustrated by the XRD structure shown in Figure 3. There is a considerable interaction of the triplet exciton on **1** with its neighboring chromophores in the film as evidenced by the fact that its $T_1 \rightarrow T_n$ absorption maximum is red-shifted by 35 nm relative to its maximum in solution. In comparison, the $S_0 \rightarrow S_1$ transition red shifts by nearly 50 nm. The red shift in the $T_1 \rightarrow T_n$ absorption maximum of **1** in the film is comparable to the 20 nm red shift in the $T_1 \rightarrow T_n$ absorption maximum of 6,13-bis[(triisopropylsilyl)ethynyl]-pentacene (TIPS-pentacene) that we observed previously in going from solution to a polycrystalline film.[7d] It is also consistent with the fact that the triplet energy of **1** is lowered by 0.14 eV in the film relative to the monomer, which is a considerable amount relative to the 0.26 eV stabilization of the singlet of **1**, indicative of a relatively strong interaction between the triplet exciton and its environment.

The triplet yield due to SF can be measured by determining the ground-state bleach immediately following ultrafast laser excitation, but prior to SF, and then observing the increase in the bleach as a second ground-state disappears as SF proceeds.[9a] This increase should be accompanied by the corresponding absorption changes resulting from formation of two triplet states. However, this method requires that the S_0 and T_1 absorption spectra are sufficiently well-resolved to distinguish readily between them over the time course of SF. Unfortunately, in the case of **1**, the S_0 and T_1 spectra strongly overlap, thus preventing such an analysis.

Thus, we developed an alternative method to determine the ^{3}*$\mathbf{1}$ yield in the film using a quantitative analysis of the nanosecond transient absorption data. As mentioned above, the number density of molecules in the film determined from X-ray crystallography is 8.44×10^{20} cm^{-3}. The excitation density ξ in the film is determined from the following equation:

$$\xi = \frac{E\lambda K(1 - 10^{-A})}{la} \tag{4}$$

where $E = 1.70 \pm 0.05$ mJ, $K = 5.034 \times 10^{15}$ J^{-1} nm^{-1}, $\lambda = 416$ nm, $A = 0.302 \pm 0.002$ at 416 nm, $l = (1.88 \pm 0.07) \times 10^{-5}$ cm, and $a = 0.785$ cm^2, so $\xi = (1.21 \pm 0.05) \times 10^{20}$ cm^{-3}. The errors on the measured quantities are the standard deviations of several measurements, and the resulting errors are arithmetically propagated to give the final errors on the derived quantities. Given that the number density of molecules in the film is $(8.44 \pm 0.01) \times 10^{20}$ cm^{-3}, an excitation density of $(1.21 \pm 0.05) \times 10^{20}$ cm^{-3} implies that 14.3 ± 0.5% of the molecules of **1** in the film are initially excited. Since the absorbance of the film at 590 nm is $A = 0.563 \pm 0.002$ (Figure 5, $A = (20\,800 \pm 50$ M^{-1} cm$^{-1}) \times (1.44$ M$) \times [(1.88 \pm 0.07) \times 10^{-5}$ cm$]$), the expected initial ΔA at 590 nm due solely to ground-state bleaching and no T−T absorption in the nsTA experiment is

dx.doi.org/10.1021/ja4053174 | J. Am. Chem. Soc. 2013, 135, 14701−14712

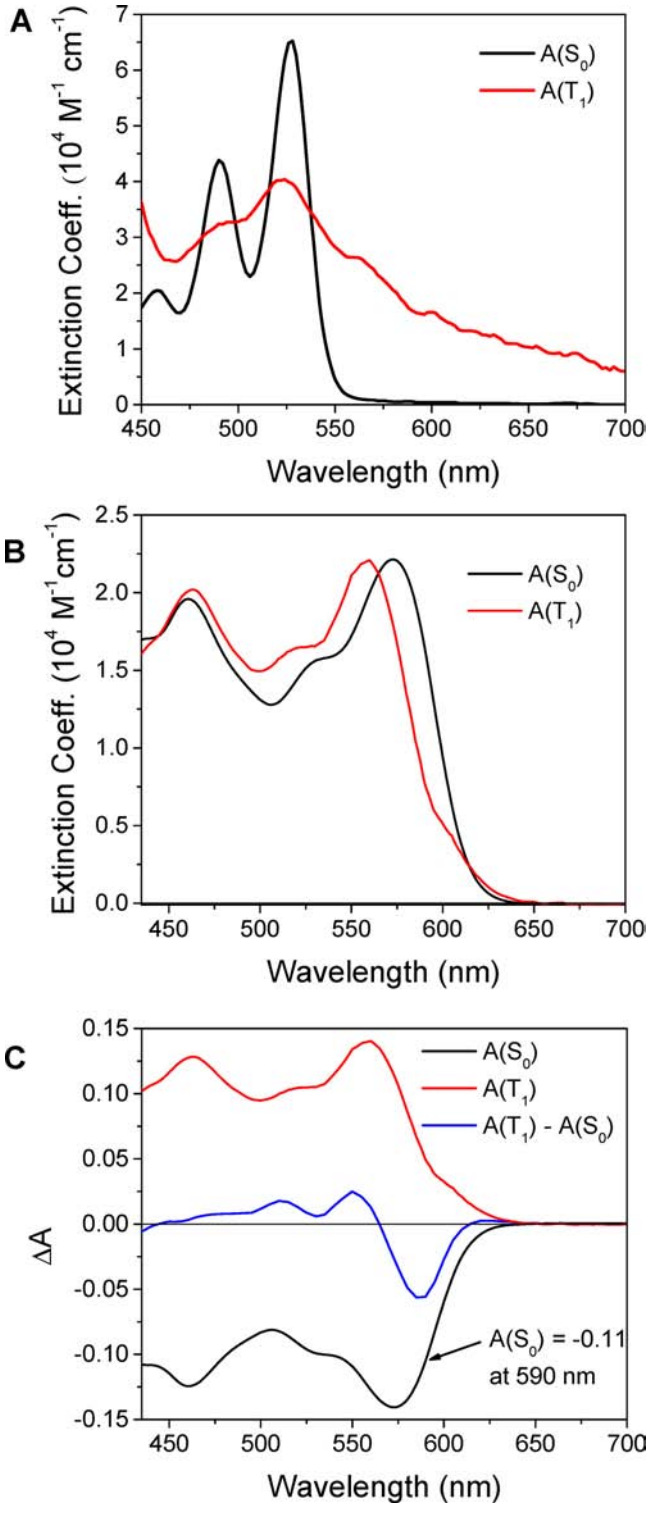

Figure 10. (A) S_0 and T_1 absorption spectra at 295 K of PDI molecule **1** (A) in toluene solution and (B) in a 188 nm film. (C) Comparison of spectra for a 188 nm thin film of **1**, where $A(S_0)$ is the amount of ground-state bleach needed to be added to the $A(T_1) - A(S_0)$ transient spectrum to obtain the triplet spectrum $A(T_1)$. See the text for an additional explanation.

$(-0.143 \pm 0.005) \times (0.563 \pm 0.002) = -0.078 \pm 0.005$. Thus, if the absorption of one photon results in the loss of only one ground-state molecule, the number of photons absorbed by the film should only produce a ground-state bleach of -0.078 ± 0.005. However, to obtain the nsTA spectrum recorded at 60 ns (Figures 9 and 10C), the total ground-state absorbance that must be subtracted from the triplet spectrum at 590 nm is 0.11 ± 0.01 (Figure 10C, $A(S_0)$ black spectrum), so the increase in required ground-state bleach means that $(-0.11 \pm 0.01)/(-0.078 \pm 0.005) = 1.4 \pm 0.2$ molecules have left the ground state, so the singlet fission yield is $140 \pm 20\%$. The ratio of ground-state bleach to triplet absorption at long times due to SF will always be 1:1 because two triplet states are produced at the expense of two ground states. This method was corroborated by successfully applying it to pentacene thin films, which undergo SF with a 200% yield (Figures S6–S9, Supporting Information),[6d,7] as well as palladium *meso*-tetraphenylporphyrin thin films, which undergo SO-ISC to produce a 100% triplet yield (Figures S10–S12, Supporting Information).[49] The main error source in this analysis is the uncertainty in subtracting the correct amount of ground-state absorption from the triplet exciton spectrum. This process is illustrated in detail for the PDI thin film in Figure S13 in the Supporting Information, where the ground-state spectrum is scaled to varying degrees and then added to the nsTA spectrum to obtain the PDI triplet spectrum.

Triplet-State Formation Mechanisms. The intrinsic triplet quantum yield of monomeric PDI is very low (<1%) because SO-ISC is slow.[25] The ultrafast 180 ps time constant for the appearance of ^{3}*1 in the polycrystalline thin films examined here is consistent with a dominant SF mechanism. Any competing triplet formation mechanisms must readily account for both the fast formation and the high triplet exciton yield in polycrystalline **1**. For example, photoinduced charge separation within electron donor–acceptor molecules frequently produces radical ion pairs in which the spin–spin exchange interaction, 2*J*, between the two radicals is sufficiently weak that radical-pair intersystem crossing (RP-ISC) takes place to yield a triplet radical ion pair, which subsequently recombines to produce the neutral triplet state of either the donor or the acceptor.[50] While symmetry-breaking within the excited singlet state of π-stacked amino-substituted PDI derivatives leading to charge separation has been observed previously when their CT states are low-lying,[21j,51] the fsTA spectra of **1** in the thin films show no evidence of $\mathbf{1}^{\bullet+}$ or $\mathbf{1}^{\bullet-}$.[52] On the basis of the measured one-electron redox potentials for formation of $\mathbf{1}^{\bullet+}$ or $\mathbf{1}^{\bullet-}$ (E_{OX} = 1.61 V and E_{RED} = −0.65 V vs SCE, respectively[53]), as well as the relatively low static dielectric constant of the largely aliphatic/aromatic molecular solid ($\varepsilon_S \cong 2.5$), the dielectric continuum model of solvation[54] predicts that photogeneration of a $\mathbf{1}^{\bullet+}$–$\mathbf{1}^{\bullet-}$ radical ion pair on adjacent molecules within the slip-stacked structure should be strongly endergonic. Moreover, even if photoexcitation of **1** within the slip-stacked columns in the polycrystalline solid could generate an energetically accessible $\mathbf{1}^{\bullet+}$–$\mathbf{1}^{\bullet-}$ radical ion pair on adjacent molecules, the value of 2*J* would mostly likely be orders of magnitude too large to permit RP-ISC.[50] Lastly, spin evolution within radical pairs centered on light elements is generally slow, on the order of 10^8–10^9 s^{-1}, so the observed time constant for ^{3}*1 formation in the polycrystalline thin film is much faster than that for RP-ISC. On the basis of our experimental observations and the weak coupling requirements of the RP-ISC mechanism, triplet exciton formation in films of **1** by this mechanism can be discounted.

Another triplet formation mechanism originally proposed by El-Sayed,[55] first noted in electron donor–acceptor molecules by Okada et al.[56] and more recently explored by Dance et al.[57]

dx.doi.org/10.1021/ja4053174 | J. Am. Chem. Soc. 2013, 135, 14701–14712

using a variety of donor−bridge−acceptor systems, relies on the large changes in orbital angular momentum characteristic of transferring electrons between orbitals of differing symmetries to induce rapid intersystem crossing in a photogenerated radical ion pair followed by charge recombination. Once again, this spin−orbit charge transfer intersystem crossing (SOCT-ISC) mechanism requires charge separation, which is not observed in films of **1** and at the same time requires the transfer to occur between orbitals having different symmetries, which is not the case in the $\pi-\pi$ slip-stacked structural relationship between individual molecules of **1** within the polycrystalline solid.

Lastly, ^{3}*$\mathbf{1}$ formation may occur via ordinary SO-ISC in excimer-like states, ^{1}*($\mathbf{1}_{A}\mathbf{1}_{B}$), where molecules A and B are adjacent within the $\pi-\pi$ slip-stacked structure.[57a,58] Previous studies on covalent PDI derivatives in which two PDI molecules are constrained to adopt a cofacial geometry show that intersystem crossing is relatively slow for ^{1}*($\mathbf{1}_{A}\mathbf{1}_{B}$), generally occurring in 5−20 ns.[58] The results presented here show that ^{3}*$\mathbf{1}$ formation occurs in high yield on an ultrafast time scale, which is consistent with an SF mechanism and not SO-ISC within an excimer-like state.

While extensive computational work has been carried out on pentacene and other SF chromophores to identify and quantify which electronic coupling matrix elements are responsible for SF,[16] there is only one report which maps out the overall electronic coupling matrix element for SF as a function of *x*,*y* translation of two parallel PDI molecules offset in the interplanar $\pi-\pi$ stacking *z*-direction by 3.5 Å.[16m] These computations predict that the SF yield has a local maximum when the degree of slippage along the N−N axis (defined as d*x* in ref 16m) is 3.5−4.0 Å and d*y* = 0.0−0.5 Å. The PXRD data for the polycrystalline films of **1** suggest that this intermolecular geometry is present in these samples, so our high SF yield in these films is consistent with this computational model.

CONCLUSIONS

The present results on molecule **1** show that its $\pi-\pi$ slip-stacked structure in the solid state produces a high SF quantum yield. Even though SF in this system is endothermic by about 0.2 eV in vapor-deposited polycrystalline thin films, the yield of ^{3}*$\mathbf{1}$ is 140 ± 20% and occurs in τ_{SF} = 180 ± 10 ps. This high yield is most likely due to the entropic effects of generating two triplet excitons, resulting in an overall exergonic process as was recently suggested for tetracene.[6b] Transient absorption and emission spectroscopies show that only singlet−singlet annihilation competes with SF at higher laser excitation densities on an ultrafast time scale and that no other competing triplet formation mechanisms are experimentally observed. Further studies using time-resolved EPR spectroscopy are being pursued to better understand the SF mechanism. On the basis of the results presented here, perylenediimide and related rylene derivatives provide an effective platform for developing an understanding of how molecular structure in the solid state determines the photophysical characteristics of these chromophores in ways that promote singlet exciton fission. This understanding will have an important impact on the use of these derivatives as photoactive materials to potentially enhance solar cell performance and charge separation in systems for artificial photosynthesis.

ASSOCIATED CONTENT

Supporting Information

Experimental details, including synthesis and surface characterization of films of **1**, additional spectroscopic data for films of **1**, pentacene, and palladium *meso*-tetraphenylporphyrin, and CIF data. This material is available free of charge via the Internet at http://pubs.acs.org.

AUTHOR INFORMATION

Corresponding Author

m-wasielewski@northwestern.edu

Notes

The authors declare no competing financial interest.

ACKNOWLEDGMENTS

This work was supported by the Chemical Sciences, Geosciences, and Biosciences Division, Office of Basic Energy Sciences, U.S. Department of Energy (DOE), under Grant Nos. DE-FG02-99ER14999 (M.R.W.) and DE-FG02-09ER16084 (S.S.). S.W.E. acknowledges support from the International Materials Institute for Solar Energy and Environment funded by the National Science Foundation under Grant No. DMR-0843962. B.S.V. is supported by the Department of Energy Office of Science Graduate Research Fellowship Program (DOE SCGF), made possible in part by the American Recovery and Reinvestment Act of 2009, administered by ORISE-ORAU (Oak Ridge Institute for Science and Education and Oak Ridge Associated Universities) under Contract No. DE-AC05-06OR23100. C.R. and T.J.M. were supported as part of the ANSER Center, an Energy Frontier Research Center funded by the Office of Basic Energy Sciences, Office of Science, U.S. DOE, under Award No. DE-SC0001059. Powder X-ray diffraction measurements were performed at the J.B. Cohen X-ray Diffraction Facility supported by the Materials Research Science and Engineering Centers (MRSEC) program of the National Science Foundation (Grant No. DMR-0520513) at the Materials Research Center of Northwestern University. We thank Dr. Amanda Smeigh for obtaining the triplet spectrum of **1** in solution and Dr. Dick Co for preliminary time-resolved spectroscopic measurements.

REFERENCES

(1) Smith, M. B.; Michl, J. *Chem. Rev.* **2010**, *110*, 6891.
(2) Hanna, M. C.; Nozik, A. J. *J. Appl. Phys.* **2006**, *100*, 074510/1.
(3) Singh, S.; Jones, W. J.; Siebrand, W.; Soticheff, B. P.; Schneider, W. *J. Chem. Phys.* **1965**, *42*, 330.
(4) (a) Swenberg, C. E.; Tracy, W. T. *Chem. Phys. Lett.* **1968**, *2*, 327. (b) Geacintov, N. E.; Burgos, J.; Pope, M.; Strom, C. *Chem. Phys. Lett.* **1971**, *11*, 504. (c) Geacintov, N. E.; Pope, M.; Vogel, F. *Phys. Rev. Lett.* **1969**, *22*, 593. (d) Groff, R. P.; Avakian, G. P.; Merrifield, R. E. *Phys. Rev. B* **1970**, *2*, 815. (e) López-Delgado, R.; Miehé, J. A.; Sipp, B. *Opt. Commun.* **1976**, *19*, 79. (f) Merrifield, R. E.; Aviakan, P.; Groff, R. P. *Chem. Phys. Lett.* **1969**, *3*, 155. (g) Pope, M.; N., G.; Vogel, F. *Mol. Cryst. Liq. Cryst.* **1969**, *6*, 83. (h) Swenberg, C. E.; Van Metter, R.; Ratner, M. *Chem. Phys. Lett.* **1972**, *16*, 482. (i) Tomkiewicz, Y.; Groff, R. P.; Avakian, P. *J. Chem. Phys.* **1971**, *54*, 4504.
(5) Von Burg, K.; Zschokke-Graenacher, I. *J. Chem. Phys.* **1979**, *70*, 3807.
(6) (a) Burdett, J. J.; Bardeen, C. J. *J. Am. Chem. Soc.* **2012**, *134*, 8597. (b) Chan, W.-L.; Ligges, M.; Zhu, X. Y. *Nat. Chem.* **2012**, *4*, 840. (c) Roberts, S. T.; McAnally, R. E.; Mastron, J. N.; Webber, D. H.; Whited, M. T.; Brutchey, R. L.; Thompson, M. E.; Bradforth, S. E. *J. Am. Chem. Soc.* **2012**, *134*, 6388. (d) Chan, W.-L.; Tritsch, J. R.; Zhu, X. Y. *J. Am. Chem. Soc.* **2012**, *134*, 18295.

(7) (a) Rao, A.; Wilson, M. W. B.; Albert-Seifried, S.; Di Pietro, R.; Friend, R. H. *Phys. Rev. B: Condens. Matter Mater. Phys.* **2011**, *84*, 195411/1. (b) Wilson, M. W. B.; Rao, A.; Clark, J.; Kumar, R. S. S.; Brida, D.; Cerullo, G.; Friend, R. H. *J. Am. Chem. Soc.* **2011**, *133*, 11830. (c) Chan, W.-L.; Ligges, M.; Jailaubekov, A.; Kaake, L.; Miaja-Avila, L.; Zhu, X. Y. *Science (Washington, DC, U. S.)* **2011**, *334*, 1541. (d) Ramanan, C.; Smeigh, A. L.; Anthony, J. E.; Marks, T. J.; Wasielewski, M. R. *J. Am. Chem. Soc.* **2012**, *134*, 386.

(8) Zenz, C.; Cerullo, G.; Lanzani, G.; Graupner, W.; Meghdadi, F.; De Silvestri, S.; Leising, G. *Synth. Met.* **1999**, *101*, 660.

(9) (a) Johnson, J. C.; Nozik, A. J.; Michl, J. *J. Am. Chem. Soc.* **2010**, *132*, 16302. (b) Schwerin, A. F.; Johnson, J., C.; Smith, M. B.; Sreearunothai, P.; Popovic, D.; Cerny, J.; Havlas, Z.; Paci, I.; Akdag, A.; MacLeod, M. K.; Chen, X.; David, D. E.; Ratner, M. A.; Miller, J. R.; Nozik, A. J.; Michl, J. *J. Phys. Chem. A* **2010**, *114*, 1457.

(10) (a) Albrecht, W. G.; Michel-Beyerle, M. E.; Yakhot, V. *Chem. Phys.* **1978**, *35*, 193. (b) Albrecht, W. G.; Michel-Beyerle, M. E.; Yakhot, V. *J. Lumin.* **1979**, *20*, 147.

(11) Katoh, R.; Kotani, M. *Chem. Phys. Lett.* **1992**, *196*, 108.

(12) (a) Najafov, H.; Lee, B.; Zhou, Q.; Feldman, L. C.; Podzorov, V. *Nat. Mater.* **2010**, *9*, 938. (b) Ryasnyanskiy, A.; Biaggio, I. *Phys. Rev. B: Condens. Matter Mater. Phys.* **2011**, *84*, 193203/1. (c) Ma, L.; Zhang, K.; Kloc, C.; Sun, H.; Michel-Beyerle, M. E.; Gurzadyan, G. G. *Phys. Chem. Chem. Phys.* **2012**, *14*, 8307.

(13) (a) Wang, C.; Tauber, M. J. *J. Am. Chem. Soc.* **2010**, *132*, 13988. (b) Wang, C.; Schlamadinger, D. E.; Desai, V.; Tauber, M. J. *ChemPhysChem* **2011**, *12*, 2891. (c) Wang, C.; Berg, C. J.; Hsu, C.-C.; Merrill, B. A.; Tauber, M. J. *J. Phys. Chem. B* **2012**, *116*, 10617. (d) Kingma, H.; Van Grondelle, R.; Duysens, L. N. M. *Biochim. Biophys. Acta, Bioenerg.* **1985**, *808*, 383. (e) Nuijs, A. M.; Van Grondelle, R.; Joppe, H. L. P.; Van Bochove, A. C.; Duysens, L. N. M. *Biochim. Biophys. Acta, Bioenerg.* **1985**, *810*, 94. (f) Alster, J.; Polivka, T.; Arellano, J. B.; Chabera, P.; Vacha, F.; Psencik, J. *Chem. Phys.* **2010**, *373*, 90.

(14) (a) Austin, R. H.; Baker, G. L.; Etemad, S.; Thompson, R. *J. Chem. Phys.* **1989**, *90*, 6642. (b) Dellepiane, G.; Comoretto, D.; Cuniberti, C. *J. Mol. Struct.* **2000**, *521*, 157. (c) Kraabel, B.; Hulin, D.; Aslangul, C.; Lapersonne-Meyer, C.; Schott, M. *Chem. Phys.* **1998**, *227*, 83. (d) Lanzani, G.; Cerullo, G.; Zavelani-Rossi, M.; De Silvestri, S.; Comoretto, D.; Musso, G.; Dellepiane, G. *Phys. Rev. Lett.* **2001**, *87*, 187402. (e) Wohlgenannt, M.; Graupner, W.; Osterbacka, R.; Leising, G.; Comoretto, D.; Vardeny, Z. V. *Synth. Met.* **1999**, *101*, 267. (f) Osterbacka, R.; Wohlgenannt, M.; Chinn, D.; Vardeny, Z. V. *Phys. Rev. B* **1999**, *60*, R11253. (g) Osterbacka, R.; Wohlgenannt, M.; Shkunov, M.; Chinn, D.; Vardeny, Z. V. *J. Chem. Phys.* **2003**, *118*, 8905.

(15) Bange, S.; Scherf, U.; Lupton, J. M. *J. Am. Chem. Soc.* **2012**, *134*, 1946.

(16) (a) Zimmerman, P. M.; Zhang, Z.; Musgrave, C. B. *Nat. Chem.* **2010**, *2*, 648. (b) Greyson, E. C.; Stepp, B. R.; Chen, X.; Schwerin, A. F.; Paci, I.; Smith, M. B.; Akdag, A.; Johnson, J. C.; Nozik, A. J.; Michl, J.; Ratner, M. A. *J. Phys. Chem. B* **2010**, *114*, 14223. (c) Paci, I.; Johnson Justin, C.; Chen, X.; Rana, G.; Popovic, D.; David Donald, E.; Nozik Arthur, J.; Ratner Mark, A.; Michl, J. *J. Am. Chem. Soc.* **2006**, *128*, 16546. (d) Zimmerman, P. M.; Bell, F.; Casanova, D.; Head-Gordon, M. *J. Am. Chem. Soc.* **2011**, *133*, 19944. (e) Quarti, C.; Fazzi, D.; Del Zoppo, M. *Phys. Chem. Chem. Phys.* **2011**, *13*, 18615. (f) Havenith, R. W. A.; de Gier, H. D.; Broer, R. *Mol. Phys.* **2012**, *110*, 2445. (g) Ito, S.; Minami, T.; Nakano, M. *J. Phys. Chem. C* **2012**, *116*, 19729. (h) Minami, T.; Ito, S.; Nakano, M. *J. Phys. Chem. Lett.* **2012**, *3*, 2719. (i) Minami, T.; Nakano, M. *J. Phys. Chem. Lett.* **2012**, *3*, 145. (j) Teichen, P. E.; Eaves, J. D. *J. Phys. Chem. B* **2012**, *116*, 11473. (k) Aryanpour, K.; Munoz, J. A.; Mazumdar, S. *arXiv.org, e-Print Arch., Condens. Matter* **2012**, 1. (l) Akdag, A.; Havlas, Z.; Michl, J. *J. Am. Chem. Soc.* **2012**, *134*, 14624. (m) Renaud, N.; Sherratt, P. A.; Ratner, M. A. *J. Phys. Chem. Lett.* **2013**, *4*, 1065.

(17) (a) Rao, A.; Wilson, M. W. B.; Hodgkiss, J. M.; Albert-Seifried, S.; Bassler, H.; Friend, R. H. *J. Am. Chem. Soc.* **2010**, *132*, 12698. (b) Jadhav, P. J.; Mohanty, A.; Sussman, J.; Lee, J.; Baldo, M. A. *Nano Lett.* **2011**, *11*, 1495. (c) Wu, S.-k.; Wang, P.-f. *Yingxiang Kexue Yu Guang Huaxue* **2011**, *29*, 1. (d) Ehrler, B.; Musselman, K. P.; Boehm, M. L.; Friend, R. H.; Greenham, N. C. *Appl. Phys. Lett.* **2012**, *101*, 153507/1. (e) Ehrler, B.; Wilson, M. W. B.; Rao, A.; Friend, R. H.; Greenham, N. C. *Nano Lett.* **2012**, *12*, 1053. (f) Huang, W.-S.; Lee, T.-H.; Guo, T.-F.; Huang, J. C. A.; Wen, T.-C. *Appl. Phys. Lett.* **2012**, *101*, 053307/1. (g) Reusswig, P. D.; Congreve, D. N.; Thompson, N. J.; Baldo, M. A. *Appl. Phys. Lett.* **2012**, *101*, 113304/1. (h) Jadhav, P. J.; Brown, P. R.; Thompson, N.; Wunsch, B.; Mohanty, A.; Yost, S. R.; Hontz, E.; Van Voorhis, T.; Bawendi, M. G.; Bulovic, V.; Baldo, M. A. *Adv. Mater. (Weinheim, Ger.)* **2012**, *24*, 6169.

(18) (a) Merrifield, R. E. *J. Chem. Phys.* **1968**, *48*, 4318. (b) Johnson, R. C.; Merrifield, R. E. *Phys. Rev. B* **1970**, *[3] 1*, 896. (c) Suna, A. *Phys. Rev. B* **1970**, *[3] 1*, 1716.

(19) Marcus, R. A. *J. Chem. Phys.* **1956**, *24*, 966.

(20) (a) Burdett, J. J.; Mueller, A. M.; Gosztola, D.; Bardeen, C. J. *J. Chem. Phys.* **2010**, *133*, 144506/1. (b) Mueller, A. M.; Avlasevich, Y. S.; Schoeller, W. W.; Müllen, K.; Bardeen, C. J. *J. Am. Chem. Soc.* **2007**, *129*, 14240. (c) Mueller, A. M.; Avlasevich, Y. S.; Müllen, K.; Bardeen, C. J. *Chem. Phys. Lett.* **2006**, *421*, 518.

(21) (a) Würthner, F.; Thalacker, C.; Sautter, A. *Adv. Mater.* **1999**, *11*, 754. (b) Langhals, H.; Saulich, S. *Chem.—Eur. J.* **2002**, *8*, 5630. (c) Schenning, A.; Herrikhuyzen, J.; Jonkheijm, P.; Chen, Z.; Würthner, F.; Meijer, E. *J. Am. Chem. Soc.* **2002**, *124*, 10252. (d) Ahrens, M. J.; Sinks, L. E.; Rybtchinski, B.; Liu, W.; Jones, B. A.; Giaimo, J. M.; Gusev, A. V.; Goshe, A. J.; Tiede, D. M.; Wasielewski, M. R. *J. Am. Chem. Soc.* **2004**, *126*, 8284. (e) Li, X. Y.; Sinks, L. E.; Rybtchinski, B.; Wasielewski, M. R. *J. Am. Chem. Soc.* **2004**, *126*, 10810. (f) Zhang, J.; Hoeben, F. J. M.; Pouderoijen, M. J.; Schenning, A. P. H.; Meijer, E. W.; Schryver, F. C.; De Feyter, S. *Chem.—Eur. J.* **2006**, *12*, 9046. (g) Rybtchinski, B.; Sinks, L. E.; Wasielewski, M. R. *J. Phys. Chem. A* **2004**, *108*, 7497. (h) Rybtchinski, B.; Sinks, L. E.; Wasielewski, M. R. *J. Am. Chem. Soc.* **2004**, *126*, 12268. (i) van der Boom, T.; Hayes, R. T.; Zhao, Y.; Bushard, P. J.; Weiss, E. A.; Wasielewski, M. R. *J. Am. Chem. Soc.* **2002**, *124*, 9582. (j) Giaimo, J. M.; Gusev, A. V.; Wasielewski, M. R. *J. Am. Chem. Soc.* **2002**, *124*, 8530. (k) You, C.-C.; Würthner, F. *Org. Lett.* **2004**, *6*, 2401. (l) Wasielewski, M. R. *J. Org. Chem.* **2006**, *71*, 5051. (m) Ahrens, M. J.; Kelley, R. F.; Dance, Z. E. X.; Wasielewski, M. R. *Phys. Chem. Chem. Phys.* **2007**, *9*, 1469. (n) Kaiser, T. E.; Wang, H.; Stepanenko, V.; Würthner, F. *Angew. Chem., Int. Ed.* **2007**, *46*, 5541. (o) Bullock, J. E.; Kelley, R. F.; Wasielewski, M. R. *PMSE Prepr.* **2007**, *96*, 805. (p) Bullock, J. E.; Carmieli, R.; Mickley, S. M.; Vura-Weis, J.; Wasielewski, M. R. *J. Am. Chem. Soc.* **2009**, *131*, 11919. (q) Kaiser, T. E.; Scheblykin, I. G.; Thomsson, D.; Würthner, F. *J. Phys. Chem. B* **2009**, *113*, 15836. (r) Marciniak, H.; Li, X.-Q.; Würthner, F.; Lochbrunner, S. *J. Phys. Chem. A* **2011**, *115*, 648. (s) Ambrosek, D.; Marciniak, H.; Lochbrunner, S.; Tatchen, J.; Li, X.-Q.; Würthner, F.; Kuehn, O. *Phys. Chem. Chem. Phys.* **2011**, *13*, 17649. (t) Würthner, F.; Kaiser, T. E.; Saha-Moeller, C. R. *Angew. Chem., Int. Ed.* **2011**, *50*, 3376. (u) Gunderson, V. L.; Krieg, E.; Vagnini, M. T.; Iron, M. A.; Rybtchinski, B.; Wasielewski, M. R. *J. Phys. Chem. B* **2011**, *115*, 7533.

(22) (a) Tang, C. W. *Appl. Phys. Lett.* **1986**, *48*, 183. (b) Ferrere, S.; Zaban, A.; Gregg, B. A. *J. Phys. Chem. B* **1997**, *101*, 4490. (c) Dittmer, J. J.; Marseglia, E. A.; Friend, R. H. *Adv. Mater.* **2000**, *12*, 1270. (d) Gregg, B. A.; Cormier, R. A. *J. Am. Chem. Soc.* **2001**, *123*, 7959. (e) Schmidt-Mende, L.; Fechtenkotter, A.; Müllen, K.; Moons, E.; Friend, R. H.; MacKenzie, J. D. *Science* **2001**, *293*, 1119. (f) Neuteboom, E. E.; Meskers, S. C. J.; van Hal, P. A.; van Duren, J. K. J.; Meijer, E. W.; Janssen, R. A. J.; Dupin, H.; Pourtois, G.; Cornil, J.; Lazzaroni, R.; Bredas, J. L.; Beljonne, D. *J. Am. Chem. Soc.* **2003**, *125*, 8625. (g) Shin, W. S.; Jeong, H.-H.; Kim, M.-K.; Jin, S.-H.; Kim, M.-R.; Lee, J.-K.; Lee, J. W.; Gal, Y.-S. *J. Mater. Chem.* **2006**, *16*, 384. (h) Kim, M. H.; Cho, M. J.; Kim, K. H.; Hoang, M. H.; Lee, T. W.; Jin, J.-I.; Kang, N. S.; Yu, J.-W.; Choi, D. H. *Org. Electron.* **2009**, *10*, 1429. (i) Woodhouse, M.; Perkins, C. L.; Rawls, M. T.; Cormier, R. A.; Liang, Z.; Nardes, A. M.; Gregg, B. A. *J. Phys. Chem. C* **2010**, *114*, 6784. (j) Hains, A. W.; Chen, H.-Y.; Reilly, T. H., III; Gregg, B. A. *ACS Appl. Mater. Interfaces* **2011**, *3*, 4381. (k) Zhan, X.; Facchetti, A.;

Barlow, S.; Marks, T. J.; Ratner, M. A.; Wasielewski, M. R.; Marder, S. R. *Adv. Mater.* **2011**, *23*, 268. (l) Liang, Z.; Cormier, R. A.; Nardes, A. M.; Gregg, B. A. *Synth. Met.* **2011**, *161*, 1014. (m) Keivanidis, P. E.; Kamm, V.; Zhang, W.; Floudas, G.; Laquai, F.; McCulloch, I.; Bradley, D. D. C.; Nelson, J. *Adv. Funct. Mater.* **2012**, *22*, 2318. (n) Raj, M. R.; Anandan, S.; Solomon, R. V.; Venuvanalingam, P.; Iyer, S. S. K.; Ashokkumar, M. *J. Photochem. Photobiol., A* **2012**, *247*, 52. (o) Rajaram, S.; Shivanna, R.; Kandappa, S. K.; Narayan, K. S. *J. Phys. Chem. Lett.* **2012**, *3*, 2405.

(23) Langhals, H.; Ismael, R. *Eur. J. Org. Chem.* **1998**, 1915.

(24) (a) Thalacker, C.; Würthner, F. *Adv. Funct. Mater.* **2002**, *12*, 209. (b) Wang, W.; Li, L. S.; Helms, G.; Zhou, H. H.; Li, A. D. Q. *J. Am. Chem. Soc.* **2003**, *125*, 1120. (c) Würthner, F. *Chem. Commun.* **2004**, 1564. (d) Yan, P.; Chowdhury, A.; Holman, M. W.; Adams, D. M. *J. Phys. Chem. B* **2005**, *109*, 724. (e) Chen, Z.; Baumeister, U.; Tschierske, C.; Würthner, F. *Chem.—Eur. J.* **2007**, *13*, 450. (f) Ghosh, S.; Li, X.-Q.; Stepanenko, V.; Würthner, F. *Chem.—Eur. J.* **2008**, *14*, 11343. (g) Dehm, V.; Buechner, M.; Seibt, J.; Engel, V.; Würthner, F. *Chem. Sci.* **2011**, *2*, 2094. (h) Xie, Z.; Stepanenko, V.; Radacki, K.; Würthner, F. *Chem.—Eur. J.* **2012**, *18*, 7060.

(25) Ford, W. E.; Kamat, P. V. *J. Phys. Chem.* **1987**, *91*, 6373.

(26) Fukuzumi, S.; Ohkubo, K.; Ortiz, J.; Gutierrez, A. M.; Fernandez-Lazaro, F.; Sastre-Santos, A. *J. Phys. Chem. A* **2008**, *112*, 10744.

(27) (a) Nantalaksakul, A.; Reddy, D. R.; Bardeen, C. J.; Thayumanavan, S. *Photosynth. Res.* **2006**, *87*, 133. (b) Muller, A. M.; Avlasevich, Y. S.; Mullen, K.; Bardeen, C. J. *Chem. Phys. Lett.* **2006**, *421*, 518. (c) Frolov, S. V.; Kloc, C.; Batlogg, B.; Wohlgenannt, M.; Jiang, X.; Vardeny, Z. V. *Phys. Rev. B: Condens. Matter Mater. Phys.* **2001**, *63*, 205203/1.

(28) Larson, A. C.; Von Dreele, R. B. *General Structure Analysis System (GSAS)*; Los Alamos National Laboratory Report LAUR 86-748; Los Alamos, NM, 2004.

(29) (a) Kelley, R. F.; Goldsmith, R. H.; Wasielewski, M. R. *J. Am. Chem. Soc.* **2007**, *129*, 6384. (b) Bullock, J. E.; Vagnini, M. T.; Ramanan, C.; Co, D. T.; Wilson, T. M.; Dicke, J. W.; Marks, T. J.; Wasielewski, M. R. *J. Phys. Chem. B* **2010**, *114*, 1794. (c) Lukas, A. S.; Miller, S. E.; Wasielewski, M. R. *J. Phys. Chem. B* **2000**, *104*, 931.

(30) Malinowski, E. R. *Factor Analysis in Chemistry*, 3rd ed.; Wiley: New York, 2002.

(31) (a) Den Hollander, W. T. F.; Bakker, J. G. C.; van Grondelle, R. *Biochim. Biophys. Acta* **1983**, *725*, 492. (b) Gillbro, T.; Sandstrom, A.; Spanfort, M.; Sundstrom, V.; van Grondelle, R. *Biochim. Biophys. Acta* **1988**, *934*, 369. (c) Bittner, T.; Irrgang, K.-D.; Renger, G.; Wasielewski, M. R. *J. Phys. Chem.* **1994**, *98*, 11821.

(32) *MATLAB*; The MathWorks, Inc.: Natick, MA, 2013.

(33) Bullock, J. E.; Carmieli, R.; Mickley, S. M.; Vura-Weis, J.; Wasielewski, M. R. *J. Am. Chem. Soc.* **2009**, *131*, 11919.

(34) *Surface Xplorer*, Ultrafast Systems LLC: Sarasota, FL, 2010.

(35) Takiff, L.; Boxer, S. G. *Biochim. Biophys. Acta* **1988**, *932*, 325.

(36) Kasha, M.; Rawls, H. R.; Ashraf El-Bayoumi, M. *Pure Appl. Chem.* **1965**, *11*, 371.

(37) Mizuguchi, J. *J. Appl. Phys.* **1998**, *84*, 4479.

(38) Mizuguchi, J.; Tojo, K. *J. Phys. Chem. B* **2002**, *106*, 767.

(39) (a) Liu, W.; Settels, V.; Harbach, P. H. P.; Dreuw, A.; Fink, R. F.; Engels, B. *J. Comput. Chem.* **2011**, *32*, 1971. (b) Zhao, H.-M.; Pfister, J.; Settels, V.; Renz, M.; Kaupp, M.; Dehm, V. C.; Würthner, F.; Fink, R. F.; Engels, B. *J. Am. Chem. Soc.* **2009**, *131*, 15660. (c) Gisslen, L.; Scholz, R. *Phys. Rev. B: Condens. Matter Mater. Phys.* **2009**, *80*, 115309/1. (d) Fink, R. F.; Seibt, J.; Engel, V.; Renz, M.; Kaupp, M.; Lochbrunner, S.; Zhao, H.-M.; Pfister, J.; Würthner, F.; Engels, B. *J. Am. Chem. Soc.* **2008**, *130*, 12858.

(40) Schubert, A.; Settels, V.; Liu, W.; Würthner, F.; Meier, C.; Fink, R. F.; Schindlbeck, S.; Lochbrunner, S.; Engels, B.; Engel, V. *J. Phys. Chem. Lett.* **2013**, *4*, 792.

(41) Giaimo, J. M.; Lockard, J. V.; Sinks, L. E.; Scott, A. M.; Wilson, T. M.; Wasielewski, M. R. *J. Phys. Chem. A* **2008**, *112*, 2322.

(42) Turro, N. J. *Modern Molecular Photochemistry*; University Science Books: Sausalito, CA, 1991.

(43) Katoh, R.; Kotani, M. *J. Chem. Phys.* **1991**, *94*, 5954.

(44) Katoh, R.; Kotani, M.; Hirata, Y.; Okada, T. *Chem. Phys. Lett.* **1997**, *264*, 631.

(45) Katoh, R.; Kotani, M. *Chem. Phys. Lett.* **1992**, *188*, 80.

(46) Katoh, R.; Kotani, M. *Chem. Phys. Lett.* **1990**, *174*, 541.

(47) (a) Furube, A.; Murai, M.; Tamaki, Y.; Watanabe, S.; Katoh, R. *J. Phys. Chem. A* **2006**, *110*, 6465. (b) Katoh, R.; Sinha, S.; Murata, S.; Tachiya, M. *J. Photochem Photobiol., A* **2001**, *145*, 23. (c) Katoh, R.; Tamaki, Y.; Furube, A. *J. Photochem. Photobiol., A* **2006**, *183*, 267.

(48) Schwoerer, M.; Wolf, H. C. *Organic Molecular Solids*; Wiley-VCH: Weinheim, Germany, 2007.

(49) Darwent, J. R.; Douglas, P.; Harriman, A.; Porter, G.; Richoux, M. C. *Coord. Chem. Rev.* **1982**, *44*, 83.

(50) (a) Closs, G. L.; Forbes, M. D. E.; Norris, J. R. *J. Phys. Chem.* **1987**, *91*, 3592. (b) Buckley, C. D.; Hunter, D. A.; Hore, P. J.; McLauchlan, K. A. *Chem. Phys. Lett.* **1987**, *135*, 307. (c) Colvin, M. T.; Ricks, A. B.; Scott, A. M.; Smeigh, A. L.; Carmieli, R.; Miura, T.; Wasielewski, M. R. *J. Am. Chem. Soc.* **2011**, *133*, 1240.

(51) Fuller, M. J.; Sinks, L. E.; Rybtehinski, B.; Giaimo, J. M.; Li, X. Y.; Wasielewski, M. R. *J. Phys. Chem. A* **2005**, *109*, 970.

(52) Gosztola, D.; Niemczyk, M. P.; Svec, W.; Lukas, A. S.; Wasielewski, M. R. *J. Phys. Chem. A* **2000**, *104*, 6545.

(53) Nakazono, S.; Easwaramoorthi, S.; Kim, D.; Shinokubo, H.; Osuka, A. *Org. Lett.* **2009**, *11*, 5426.

(54) Weller, A. *Z. Phys. Chem.* **1982**, *133*, 93.

(55) El-Sayed, M. A. *J. Chem. Phys.* **1974**, *60*, 4502.

(56) Okada, T.; Karaki, I.; Matsuzawa, E.; Mataga, N.; Sakata, Y.; Misumi, S. *J. Phys. Chem.* **1981**, *85*, 3957.

(57) (a) Dance, Z. E. X.; Mickley, S. M.; Wilson, T. M.; Ricks, A. B.; Scott, A. M.; Ratner, M. A.; Wasielewski, M. R. *J. Phys. Chem. A* **2008**, *112*, 4194. (b) Dance, Z. E. X.; Mi, Q.; McCamant, D. W.; Ahrens, M. J.; Ratner, M. A.; Wasielewski, M. R. *J. Phys. Chem. B* **2006**, *110*, 25163.

(58) Veldman, D.; Chopin, S. M. A.; Meskers, S. C. J.; Groeneveld, M. M.; Williams, R. M.; Janssen, R. A. J. *J. Phys. Chem. A* **2008**, *112*, 5846.